Int. J. Heat Mass Transfer. Vol. 35, No. 10, pp. 2501–2513, 1992
Printed in Great Britain

0017–9310/92 $5.00 + 0.00

A numerical study of the flow and heat-transfer characteristics of an impinging laminar slot-jet including crossflow effects

SAMI AL-SANEA

Department of Mechanical Engineering, College of Engineering, King Saud University, P.O. Box 800, Riyadh 11421, Saudi Arabia

(*Received* 26 *February* 1991 *and in final form* 29 *September* 1991)

Abstract—A numerical model, based on the finite-volume procedure, is constructed and applied for calculating the steady flow and heat-transfer characteristics of a laminar slot-jet impinging on an isothermal flat surface. Three cases are studied; namely, free-jet impingement, semi-confined-jet impingement and semi-confined-jet impingement through a crossflow. The model is validated by comparing results with available experimental data for the case of a free-jet impingement; the agreement is found to be very good. A parametric investigation is carried out by varying the following parameters: the jet Reynolds number, the fluid Prandtl number, the length of the heat-transfer surface, the jet-exit to impingement-surface distance and, in the case of a crossflow, the crossflow-to-jet mass-flow-rate ratio. The average Nusselt number is correlated for the range of parameters studied and show that the crossflow can degrade the nominal heat-transfer rate by as much as 60%.

1. INTRODUCTION

1.1. *The problem considered*

THIS paper describes the construction and application of a numerical model for simulating the hydrodynamic and thermal characteristics of a laminar, slot-jet impinging on a heated plate. The study is conducted under the effects of varying both geometrical configurations and flow conditions.

Figure 1 gives a schematic representation of the physical situations studied. The free-jet impingement case is depicted in Fig. 1(a). A free, laminar and plane jet discharges vertically downwards onto a flat heated surface of uniform temperature. A fluid can be freely entrained into the issuing jet from the ambient surroundings, the temperature of which is equal to that of the jet. Figure 1(b) presents the case of a jet impingement in a semi-confined environment. A wall, parallel to the impingement surface, is now located at the level of the jet exit plane. This wall prevents entrainment from the ambient and would, ultimately, confine the fluid to flow between two parallel plates. In the third case, as seen in Fig. 1(c), a crossflow is imposed on the left boundary of the physical domain. This crossflow, whose temperature is equal to that of the jet, combines with the jet flow and alters the flow pattern. This would give rise to different heat-transfer characteristics on the impingement surface.

The three configurations, (a), (b) and (c), presented in Fig. 1 describe three distinguished cases of impinging jets. Experimental data are available only for case (a) with which model predictions will be compared. While case (b) studies the effects of semi confinement on the slot-jet impingement behaviour, case (c) studies the resulting effects of a crossflow. With symmetric flow and temperature conditions imposed at the slot-jet exit plane, symmetric behaviour across the geometrical centre-plane arises and is taken advantage of in the calculations for the first two cases. Due to the crossflow, the third case lacks symmetry and the whole physical domain must be solved for. The geometrical parameters (l, z and b), the flow velocity and fluid properties, as well as the shape of the inlet

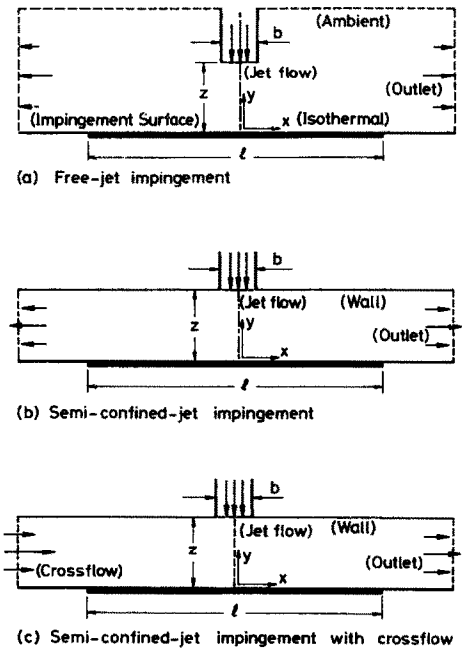

FIG. 1. Schematic representation of the physical situations studied (not to scale).

NOMENCLATURE

A a general coefficient in the finite-difference equations
b width of the slot-jet
C_f local skin-friction coefficient, $\tau_w/\frac{1}{2}\rho v_j^2$
h local heat-transfer coefficient
h_{av} average heat-transfer coefficient over L
IX, IY finite-difference grid lines in the X- and Y-directions, respectively
k thermal conductivity
l length of the heat-transfer surface
L dimensionless length, l/b
m mass flow rate
M crossflow-to-jet mass-flow-rate ratio, m_c/m_j
n, s, e, w locations midway between grid nodes
N, S, E, W, P finite-difference-grid nodes
Nu local Nusselt number, hb/k
Nu_{av} average Nusselt number, $h_{av}b/k$
NX, NY number of finite-difference-grid nodes in the X- and Y-directions, respectively
p pressure
P dimensionless pressure, $(p-p_\infty)/\rho v_j^2$; also a finite-difference-grid node
Pr Prandtl number
r length of top-wall recirculation region
R dimensionless length, r/b
Re_j Reynolds number at jet exit, $v_j b/\nu$
S source term
T temperature
u velocity component in x-direction
U dimensionless velocity component in X-direction, u/v_j
v velocity component in y-direction
V dimensionless velocity component in Y-direction, v/v_j
x coordinate along the plate from the jet axis
X dimensionless coordinate along the plate, x/b
y coordinate normal to the plate
Y dimensionless coordinate normal to the plate, y/b
z distance between jet-exit and impingement-surface
Z dimensionless distance, z/b.

Greek symbols

Γ dimensionless diffusion coefficient
Θ dimensionless temperature, $(T-T_j)/(T_w-T_j)$
μ dynamic viscosity
ν kinematic viscosity
ρ density
τ local shear stress
Φ a general dependent variable.

Subscripts

c crossflow
j slot-jet exit
N, S, E, W, P finite-difference-grid nodes
w impingement wall
Φ a general dependent variable
∞ free stream.

profiles are the key parameters that affect the flow and heat-transfer characteristics of the cases considered.

1.2. *Practical relevance*

Impinging jets are of great practical interest in many industrial areas. They are applied in turbine blade cooling, electronic components cooling, annealing of non-ferrous sheet metals, tempering of glass and drying of textiles, wood and paper. Compared to other conventional methods, impinging jets are generally used to increase the rate of heat transfer between a fluid and a solid, and are quite often employed to produce enhanced and controlled localized cooling or heating effects on surfaces. Impinging jets have, therefore, been studied extensively. The studies have, in the main, been concerned with circular jets or with relatively high velocities so that the flow is turbulent at the jet exit. The case of impingement heat transfer with a plane jet that is laminar has received less attention. Practically no attention has been given to the latter case with a crossflow effect. This is reflected quite clearly in the literature as is reviewed next. The present study is, therefore, concerned with laminar impinging slot-jets and, also, investigates the effects of a crossflow. Impingements in the presence of a crossflow are encountered quite frequently in practice as the result of, for example, the exhausting flow of upstream impinging jets.

1.3. *Review of previous work*

An early and detailed measurement of the heat-transfer coefficients between a flat plate and impinging 2-D slot-jets was carried out by Gardon and Akfirat [1]. Single and arrays of free air jets in laminar and turbulent flow conditions were studied. However, shapes of the inlet velocity profiles were not given.

Korger and Krizek [2] used the naphthalene sublimation technique to measure the mass-transfer coefficients for flow from a slotted nozzle and a system of three nozzles impinging on a flat plate. The free-

air jets were, however, mainly turbulent at the exit. Sparrow and Wong [3] used a similar measuring technique but for jets that were laminar and fully developed at exit. The heat–mass transfer analogy was used to convert the mass-transfer results into the heat-transfer counterparts. They found that the shape of the velocity profile at the jet exit had a significant effect on the transfer characteristics of the impingement surface.

On a flat surface covered with a swollen polymer coating, Masliyah and Nguyen [4] utilized a holographic interferometry technique to measure the mass-transfer coefficients for an impinging slot laminar air jet. The local Sherwood number was correlated to jet Reynolds number and distance along the surface.

Elbanna and Sabbagh [5] carried out measurement and flow visualization of the flow field resulting from the interaction of two slot-jets impinging on the ground. The jets, as applied to VTOL aircraft, were turbulent and the measurements have shown that the presence of an unequal-strength jet could highly affect the hydrodynamic characteristics at the impingement region.

On the theoretical side, one of the early numerical solutions to the problem of plane jet impinging on a heated wall was produced by Gosman *et al.* [6]. They used the vorticity and stream function method and solved the laminar and turbulent flow cases for different Prandtl numbers. Using the same computational procedure, van Heiningen *et al.* [7] studied the effects of suction and nozzle exit velocity profile on the flow and heat-transfer characteristics of a semi-confined laminar impinging slot-jet. Uniform suction at the impingement surface was shown to enhance the heat-transfer rates by a constant amount. The stagnation heat-transfer rate for a parabolic inlet velocity profile was calculated to be 1.5–2.0 times the value produced by a flat velocity profile.

Miyazaki and Silberman [8] used the potential flow solution coupled with a numerical solution of the boundary-layer equations to evaluate the local friction factor and Nusselt number of an impinging laminar jet with a uniform velocity profile at exit. Using a similar approach, Sparrow and Lee [9] investigated the effects of a non-uniform velocity profile at the jet exit on the impingement characteristics.

Mikhail *et al.* [10] performed finite-difference numerical calculations of the flow and heat-transfer characteristics of laminar jets issuing from a row of slots and impinging normally on a flat plate. The results showed that the average Nusselt number increases with the decrease in the nozzle spacing. By using a similar approach, Yuan *et al.* [11] presented numerical predictions of the effects of buoyancy on a laminar slot-jet impinging on a flat surface. For high Richardson numbers, both buoyancy assisted and retarded flows were shown to have significant effects on the enhancement and degradation, respectively, of the local Nusselt number. By employing a numerical marching finite-difference procedure, Garg and Jayaraj [12] solved the laminar boundary-layer flow for a slot-jet impinging on an inclined flat plate. They found that the local Nusselt number and skin friction coefficient could attain large values close to the stagnation point at small angles of impingement.

Cooper [13] studied the problem of heat transfer to walls from fire plume-driven ceiling jets during compartment fires. An analogy was drawn between a plane free-jet impingement on a surface and the ceiling-jet flow impingement on a compartment wall. Using the analogy, he estimated that the heat transfer rate to walls could be enhanced by a factor of 2.3 over that to ceilings.

In a literature survey on the heat-transfer characteristics of impinging jets, Downs and James [14] summarized the findings of a large number of studies. The number of studies surveyed on laminar and slot-jet impingements were much fewer than those surveyed on the turbulent and round jets. With regard to the former studies with a crossflow effect, none has appeared in the survey.

To summarize the present review, one may conclude that the studies on the laminar slot-jet impingement with a crossflow effect are very scarce despite a plentiful number of practical applications of the problem.

1.4. *Objectives of the study*

(i) To construct a mathematical model for simulating the behaviour of an impinging laminar slot-jet on a heated surface.

(ii) To apply the model to simulate three cases: (a) free-jet impingement; (b) semi-confined-jet impingement; and (c) semi-confined-jet impingement with a crossflow effect.

(iii) To validate the model by comparing predictions with available experimental measurements.

(iv) To carry out a parametric study to investigate the effects of geometry, flow conditions and fluid properties on the heat-transfer characteristics.

2. MATHEMATICAL FORMULATIONS

2.1. *Basic assumptions*

The flow and heat-transfer processes are considered to be laminar, two-dimensional and steady. The fluid properties are assumed constant and the viscous dissipation is neglected.

2.2. *The governing differential equations solved*

Subject to the above assumptions and for Cartesian coordinates, the governing equations in dimensionless form are:

Conservation of mass

$$\frac{\partial U}{\partial X}+\frac{\partial V}{\partial Y}=0. \tag{1}$$

Conservation of U-momentum

$$\frac{\partial}{\partial X}(U^2)+\frac{\partial}{\partial Y}(UV)-\frac{1}{Re_j}\left(\frac{\partial^2 U}{\partial X^2}+\frac{\partial^2 U}{\partial Y^2}\right)=-\frac{\partial P}{\partial X}. \quad (2)$$

Conservation of V-momentum

$$\frac{\partial}{\partial X}(UV)+\frac{\partial}{\partial Y}(V^2)-\frac{1}{Re_j}\left(\frac{\partial^2 V}{\partial X^2}+\frac{\partial^2 V}{\partial Y^2}\right)=-\frac{\partial P}{\partial Y}. \quad (3)$$

Conservation of energy

$$\frac{\partial}{\partial X}(U\Theta)+\frac{\partial}{\partial Y}(V\Theta)-\frac{1}{Re_j Pr}\left(\frac{\partial^2 \Theta}{\partial X^2}+\frac{\partial^2 \Theta}{\partial Y^2}\right)=0. \quad (4)$$

The dimensionless quantities used in the above equations are defined as:

$$X=x/b,\quad Y=y/b,\quad U=u/v_j,\quad V=v/v_j,$$

$$\Theta=(T-T_j)/(T_w-T_j),\quad Re_j=\rho v_j b/\mu,\quad \text{and}$$

$$P=(p-p_\infty)/\rho v_j^2.$$

The general form of transport equation.

The above set of equations can be represented by a single equation of the form:

$$\frac{\partial}{\partial X}(U\Phi)+\frac{\partial}{\partial Y}(V\Phi)-\frac{\Gamma_\Phi}{Re_j}\left(\frac{\partial^2 \Phi}{\partial X^2}+\frac{\partial^2 \Phi}{\partial Y^2}\right)=S_\Phi \quad (5)$$

where, Φ is the general variable and stands for 1, U, V and Θ in equations (1)–(4), respectively; Γ_Φ is the dimensionless exchange (diffusion) coefficient and stands for 0, 1, 1 and $1/Pr$ in equations (1)–(4), respectively; and S_Φ is the source term and represents the RHS in the equation set for Φ.

This general form of transport equation facilitates the use of the same solution procedure to be applied to all equations.

2.3. *Boundary conditions*

Inlet(s). The required distributions of both velocity components and temperature are prescribed at the slot-jet exit plane. In the present study: $U=0$, $V=1$ (either uniform or parabolic with a mean value of 1), and $\Theta=0$. In the presence of a crossflow, a fully developed parabolic velocity profile is imposed at the crossflow inlet plane which is located at 20 slot widths upstream of the slot-jet axis. This is to ensure a natural interaction of a fully developed crossflow with the jet flow. The crossflow temperature is set to $\Theta=0$.

Outlet. The outlet boundary is located far enough downstream for conditions to be substantially developed. Accordingly, the following conditions are imposed: $V=\partial U/\partial X=\partial\Theta/\partial X=0$.

Wall(s). All walls are stationary and impervious and, hence, $U=V=0$. Normal gradients of temperature are set to zero at the adiabatic walls; for the isothermal part of the impinging surface (over the length of the heat-transfer region, l), the temperature is set to $\Theta=1$.

Plane of symmetry. Symmetric conditions are imposed on the plane over the slot-jet axis; namely, $U=\partial V/\partial X=\partial\Theta/\partial X=0$. This symmetry is destroyed in the presence of a crossflow and the whole physical domain must be solved for.

Free stream. This condition is pertinent only to the case of a free-jet impingement. Here, the top boundary is located far enough above the slot-jet exit plane for the flow to assume quiescent free-stream conditions. The free-stream temperature is set to $\Theta=0$.

The proper locations of the outlet and free-stream boundaries depend on the flow situation and are determined by numerical experiments. It is found that the jet Reynolds number and the jet-exit to impingement-surface distance play a significant role in determining the size of the calculation domain. This will be elaborated along with other computational details in the Appendix.

2.4. *Closure*

There are four dependent variables that characterize the modelling of the aforementioned jet-impingement situations. These are the two velocity components U and V, the pressure P and the temperature Θ. The elliptic differential equations (1)–(4) are used to solve for these variables using the appropriate boundary conditions. A suitable numerical solution procedure is employed to perform this task as is described next.

With regard to the initial conditions, the velocities are assigned initial uniform values that satisfy the overall continuity requirement. The initial temperature field is set at the mean value of the isothermal-wall and jet-inlet temperatures.

3. THE NUMERICAL SOLUTION PROCEDURE

3.1. *Introduction*

The mathematical model uses a control-volume finite-difference method for discretizing the governing conservation equations and employs an upwind-difference scheme. The numerical solution is based on the well-known SIMPLE pressure-correction algorithm of Patankar and Spalding [15], but differs from SIMPLE in the way the finite-difference equations are solved. In SIMPLE, the dependent variables are solved one at a time for the whole flow field; in the present method, this is done on a line-by-line manner as will be outlined in Section 3.4. The computer program used and modified to suit the current jet-impingement problems is the 2/E/FIX code of Pun and Spalding [16]. Al-Sanea *et al.* [17] have briefly described and applied the line-by-line procedure in computing recirculating flows with heat transfer. The scheme was found particularly beneficial for flows where relatively large parabolic or nearly parabolic regions exist alongside the elliptic flow regions. Due to space limitations, only the essential features of the

numerical solution procedure are given. The above cited references [15–17] and, for example, Patankar [18] may be referred to for more details.

3.2. *The finite-difference grid*

The grid consists of a set of orthogonally intersecting straight lines. The points of intersection (grid nodes) provide reference locations for identifying the variables. Figure 2 shows a portion of such a grid and a typical cell enclosing node P. Point P, the central node, has four neighbouring nodes N, S, E, and W at which the pressure and temperature values are stored. The velocities are calculated and stored, as indicated by the arrows, at points midway between these grid nodes, i.e. at the cell faces identified by n, s, e and w. This grid arrangement is known as a staggered-grid system. The grid spacings need not necessarily be uniform but can vary so that it is possible to locate more grid nodes in regions with steep variation of flow properties; namely, near the impingement surface and jet axis.

Grid independent results are achieved by obtaining solutions with an increasing number of grid nodes until a stage is reached where the solution exhibits negligible change with further increase in the number of nodes. A typical study of such a finite-difference-grid independence check will be presented in Section 4.5.2. More details on the grid size and distribution are given in the Appendix.

3.3. *The finite-difference equations*

The general finite-difference equation (f.d.e.), linking the value of the variable Φ at node P to those at nodes N, S, E and W, is obtained by integrating the differential equation (5) over the volume of the finite-difference cell to yield:

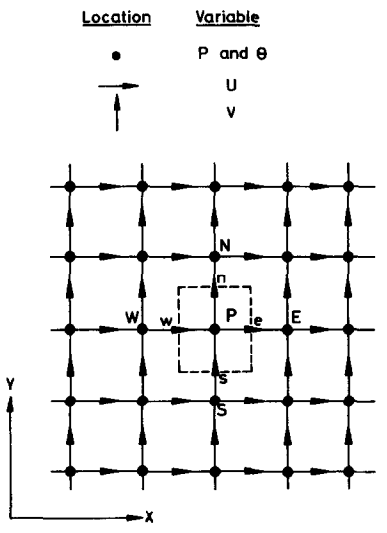

FIG. 2. A typical portion of the finite-difference grid showing location of variables and a typical node P.

$$A_P^\Phi \phi_P = A_N^\Phi \phi_N + A_S^\Phi \phi_S + A_E^\Phi \phi_E + A_W^\Phi \phi_W + S_P^\Phi \quad (6)$$

where,

$$A_P^\Phi = A_N^\Phi + A_S^\Phi + A_E^\Phi + A_W^\Phi - S_P^{\Phi\prime}. \quad (6')$$

The details of this transformation can be found in refs. [15–18] as, indeed, the setting up of the f.d.e.s for the pressure correction needed in SIMPLE.

The source term S_Φ in equation (5) has been linearized as follows:

$$S_\Phi = S_P^\Phi + S_P^{\Phi\prime}\Phi_P. \quad (7)$$

The coefficients A_N^Φ, A_S^Φ, A_E^Φ and A_W^Φ are the finite-difference coefficients and contain the effects of convection and diffusion.

The total number of f.d.e.s solved is equal to the number of the dependent variables multiplied by the number of the finite-difference cells in the flow domain. There is one such f.d.e. as equation (6) for every variable at each cell.

3.4. *Solution of the finite-difference equations*

The above f.d.e.s are coupled and non-linear due to the fact that the coefficients are functions of the dependent variables themselves. The solution is usually obtained after a number of iterations of the field and by re-evaluating the values of the coefficients every iteration. In the present program, the f.d.e.s are solved simultaneously on a line-by-line basis by the Tri-Diagonal Matrix Algorithm (TDMA). While Φ values on a line are being solved, Φ values on both sides of the line are kept unchanged. This is repeated for all variables before the next line is visited. The main solution steps can be summarized as follows:

(i) Guess values of the variables in the field.

(ii) Compute values of U by solving the f.d.e.s for the U-momentum on a line.

(iii) Compute values of V as in (ii) above.

(iv) Compute values of Θ on the line.

(v) Compute values of pressure correction on the line. The line arrangement necessitates that the pressure corrections on both sides of the line are taken to be zero.

(vi) Correct pressures and velocities on the line.

(vii) Move to the next line and repeat steps (ii)–(vi) for the whole field.

(viii) Repeat iterating the field until convergence.

The above basic cycle of operations is often modified to incorporate devices such as multiple traverse of lines and block adjustments of variables in order to enhance the convergence rate.

4. PRESENTATION AND DISCUSSION OF THE RESULTS

4.1. *Introduction*

The mathematical model presented in the previous sections is implemented in the computer code and applied to simulate the jet-impingement problems of

Fig. 1. The model is validated by comparing predictions with available experimental measurements. A parametric study is carried out by varying one parameter at a time, while keeping the rest of parameters at pre-determined default values.

4.2. *Parameters studied*

The following parameters are varied and, hence, their effects on the flow and heat-transfer characteristics are determined:

(i) The slot-jet Reynolds number (Re_j) in the range: $50 \leqslant Re_j \leqslant 450$.

(ii) The Prandtl number of the fluid (Pr) in the range: $0.1 \leqslant Pr \leqslant 100$.

(iii) The length of the heat-transfer surface (l) in the range: $6.5 \leqslant L = l/b \leqslant 20$.

(iv) The separation distance between the slot-jet exit plane and impingement surface (z) in the range: $1 \leqslant Z = z/b \leqslant 16$.

(v) The crossflow-to-jet mass-flow-rate ratio (m_c/m_j) in the range: $0.25 \leqslant M = m_c/m_j \leqslant 6$. This parameter is applicable only to the case of jet impingement through a crossflow.

The flow properties also depend on the inlet profile shapes of velocity and temperature for both jet and crossflow. For a specified geometrical configuration, inlet velocity profiles and for identical crossflow and jet temperatures, the average Nusselt number (Nu_{av}) will have a functional dependence with the following dimensionless parameters:

$$Nu_{av} = f(Re_j, Pr, L, Z, M). \quad (8)$$

Based on the characteristics of impinging jets and geometric similarity, Metzger and Korstad [19] presented a similar functional dependence in their experimental study of a single line of circular air jets impingement through a crossflow.

4.3. *Default values of parameters*

The results are presented and correlated in terms of the independent effects of Re_j, Pr, L, Z and M on Nu_{av}. Unless otherwise specified, the rest of the parameters will assume the following default values:

$$Re_j = 200, \quad Pr = 0.71, \quad L = 20,$$
$$Z = 4 \quad \text{and} \quad M = 1.0 \quad \text{or} \quad 0.$$

The velocity profile is uniform at the jet exit and that for the crossflow at inlet is always fully developed parabolic.

4.4. *Form of presentation*

The results are presented in Figs. 3–12. Emphasis is given on both the local Nusselt number (Nu) variations over the impingement surface and on the average Nusselt number (Nu_{av}) for the whole heat-transfer surface. Section 4.5.1 is devoted to the free-jet impingement results which are presented in Fig. 3. Section 4.5.2 is concerned with the results of the semi-confined-jet impingement without a crossflow effect. Figures 4 and 5 study the influence of semi-confinement and the effects of using a different size of finite-difference grids on the impingement-surface heat-

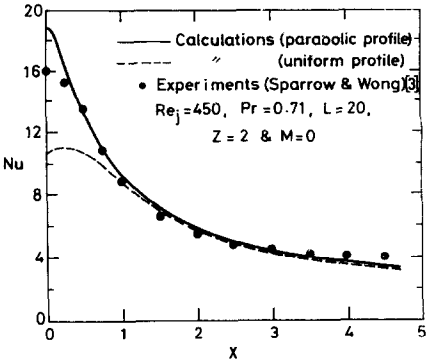

FIG. 3. Nusselt number variation along the plate; free-jet impingement showing effects of inlet velocity profile and comparisons with experimental data.

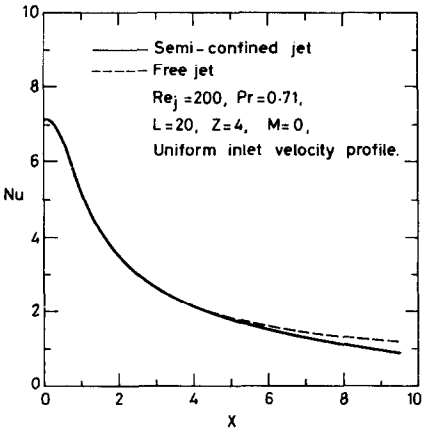

FIG. 4. Nusselt number variation along the plate; semi-confined-jet impingement showing comparisons with free-jet impingement.

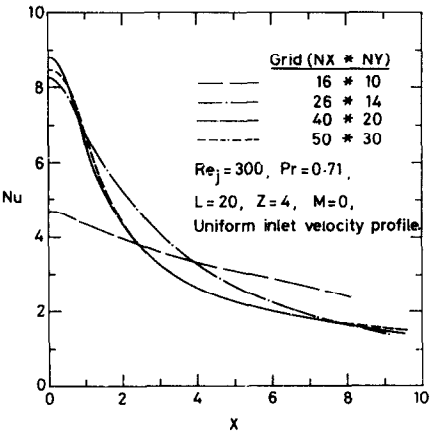

FIG. 5. Nusselt number variation along the plate; semi-confined-jet impingement showing effects of finite-difference-grid size.

transfer characteristics. Other results are displayed in subsequent figures for comparison with those with a crossflow effect. Section 4.5.3 concentrates on the results of the semi-confined-jet impingement through a crossflow. The results are presented in Figs. 6–12 and study the influence of the various parameter concerned.

4.5. *Discussion of the results*

4.5.1. *Free-jet impingement.* This problem is specified in Fig. 1(a) and is presently studied for $Re_j = 450$, $Pr = 0.71$, $L = 20$, $Z = 2$ and $M = 0$. The departure from the default values for Re_j and Z was necessitated by the available experimental measurements. The results are presented in Fig. 3 which depicts the variations of Nu with X. The continuous and dashed lines represent calculations with fully developed parabolic and uniform jet-inlet velocity profiles, respectively. The symbols correspond to the experimental measurements of Sparrow and Wong [3] who used a developed slot-jet flow impinging on a naphthalene plate. They employed the heat-mass transfer analogy to convert the results.

With the parabolic inlet velocity profile, Nu exhibits a maximum value at the stagnation point; sharp decrease follows where, at $X = 1$, Nu reaches less than half of its value at the stagnation point. Gradual reduction in Nu then continues along the heat-transfer surface. This arises from a decrease in wall temperature gradients as a consequence of thermal boundary layer development and thickening with X. It is clear that impinging jets do have the advantage of producing, at the stagnation region, a high heat flux between a fluid and a surface at different temperatures.

It is interesting to note the substantial drop in Nu at the stagnation point, which amounts here to about 45%, when an ideal uniform inlet velocity profile is used. Previous results by others had shown the same effect [7, 9, 10]. This is attributed to the fact that the velocity and momentum of the issuing jet are higher at the jet centre for the parabolic profile. However, the results of the two profiles nearly coincide with each other for $X > 1$. This suggests that after a short distance downstream of the impingement region, the flow behaves like a wall jet and is not affected substantially by its initial velocity profile.

As to the comparisons with the available measurements using a developed slot-jet flow, the agreement is in general very good. This is, of course, bearing in mind the inexact nature of the heat-mass transfer analogy involved, and also the likely differences in the theoretical and experimental jet-inlet velocity profiles.

4.5.2. *Semi-confined-jet impingement without a crossflow.* This problem is specified in Fig. 1(b) and is studied for $M = 0$ to provide benchmark results for comparisons with identical corresponding cases but with a crossflow effect. However, this will be postponed to the next section; the aim of the present section is to investigate the effects of semi-confinement and computational grid refinements. These results are displayed in Figs. 4 and 5, respectively.

For the default parameters employed, it is interesting to note from Fig. 4 that Nu values over the impingement surface and for $X < 5$ are identical for the two cases of free-jet and semi-confined-jet impingement. This suggests that the impingement region is being fully dominated by the characteristics of the issuing jet, and that the conditions prevailing at the top boundary of the domain have very little effects. Gosman *et al.* [6] have also found that, for $Re_j = 450$, $Pr = 1$ and $Z = 1$, the influence of the conditions imposed at the free boundary on the impingement characteristics was very small. Downstream of the impingement region and for $X > 5$, the model predicts, for the free-jet impingement case, values of Nu that are slightly higher than those calculated for the semi-confined-jet impingement. This is attributed to the ambient fluid entrained into the body of the issuing free jet.

Figure 5 studies the effects of using four different sizes of finite-difference grids on Nu variation along the plate. An optimum grid is determined with $Re_j = 300$ which represents an average value in the range studied. It is clear that the two coarsest grids used show results that have substantial grid effects and, hence, lack accuracy. The two finest grids employed produce results that are very close to each other and it is expected that further grid refinements would not increase the accuracy much further. It is regarded, therefore, that the grid of $NX = 40$ by $NY = 20$ gives the best compromise as far as both accuracy and computer cost are concerned. It is to be emphasized that more grid points are packed near the impingement surface and jet axis. The distribution of grid lines is tabulated in the Appendix which also contains other relevant details.

4.5.3. *Semi-confined-jet impingement with a crossflow.* This problem is specified in Fig. 1(c) and is studied to assess the crossflow effects on the impingement heat-transfer characteristics. The parameters varied and default values are given in Sections 4.2 and 4.3. The results are presented in Figs. 6–12 and are compared with the corresponding cases for $M = 0$.

(a) *Effects of crossflow on impingement-surface characteristics*

Figure 6 shows the effects of imposing different crossflow-to-jet mass-flow-rate ratios (M) on Nu variations along the plate. Due to crossflow effects, the results show asymmetry on either side of the jet geometrical centre-line ($X = 0$). For the parameters studied, the impingement point is moved downstream by about one to two slot widths. As a result of the crossflow, Nu is substantially degraded at the impingement region; elsewhere, Nu increases with the increase in the crossflow velocity. It is clear that the heat-transfer characteristics shown arise from combined effects of jet impingement and crossflow. Starting from the beginning of the heated region ($X = -10$),

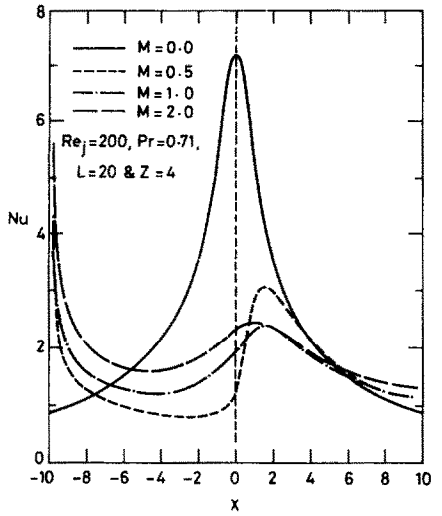

FIG. 6. Nusselt number variation along the plate; semi-confined-jet impingement with crossflow showing effects of crossflow-to-jet mass-flow-rate ratio.

Nu decreases with X as the thermal boundary layer develops; due to the effects of the impinging jet, *Nu* increases and then decreases with X as the combined streams start to develop further downstream into a parallel-to-plate flow.

Figure 7 illustrates the variations of the skin-friction coefficient (C_f) along the plate. For $M = 0$ and $X = 0$, $C_f = 0$ since this corresponds to the stagnation point; the negative values of C_f correspond to velocities opposite to the X-direction. The maximum skin-friction coefficient occurs at $X = 1$. The drop in C_f down to about zero at $X = 10$ indicates that the flow at the bottom wall is on the verge of separation. A minute separation bubble, the height of which is not much greater than 1% of the slot-jet width, is calculated at $X = 11$ (not shown). Had a coarser finite-difference grid been used, this tiny separation region on the bottom wall would have not been captured. Very shortly afterwards the flow re-attaches on the wall as it continues its development between the two parallel plates. This localized behaviour is attributed to the flow conditions prevailing outside the wall-jet region. As will be discussed in more detail in the Appendix, a big recirculation region adjacent to the top wall and above the wall-jet region is created as the jet issues from the slot, and it is after several slot widths downstream that the flow begins to re-attach on the top wall. The present wall-jet behaviour is being emphasized on since it differs from the wall-jet development under ideal conditions.

The presence of the crossflow has the tendency of suppressing small recirculation zones. The C_f values for $M > 0$ and the parameters shown in Fig. 7 indicate no flow separation on the bottom plate. It is also interesting to note that C_f remains constant until about four slot widths upstream of the jet centre-line ($X = -4$). This is due to the fully developed flow imposed at the crossflow inlet ($X = -20$). The increase in C_f from about $X = -4$ to $X = 2$ is caused by the jet flow which joins the crossflow and increases the velocity parallel to the surface. The subsequent decrease in C_f, for $X > 2$, is due to the flow development that follows over the flat surface.

(b) *Effects of jet-Reynolds-number on average Nusselt number*

The total heat-transfer rate between the flow and the plate is related to the average heat-transfer coefficient (h_{av}) which is best represented by the average Nusselt number (Nu_{av}). Figure 8 depicts the variation of Nu_{av} with Re_j for the two cases of without and with crossflow. All the other parameters are set at the default values. The average Nusselt number Nu_{av} increases with increasing Re_j but, as the calculations show, at a slower rate in the presence of a crossflow. The crossflow with $M = 1$ reduces Nu_{av} by about 20% at $Re_j = 100$; and at $Re_j = 450$, the reduction is about 40% of the nominal values. For

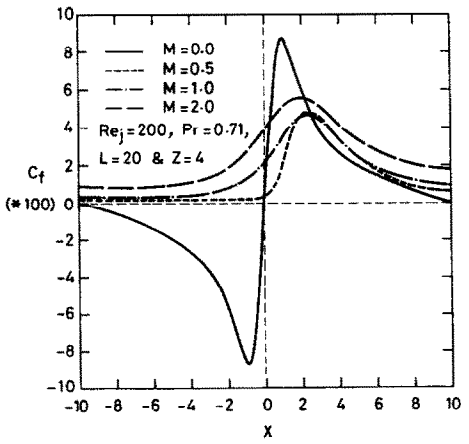

FIG. 7. Skin-friction coefficient variation along the plate; semi-confined-jet impingement with crossflow showing effects of crossflow-to-jet mass-flow-rate ratio.

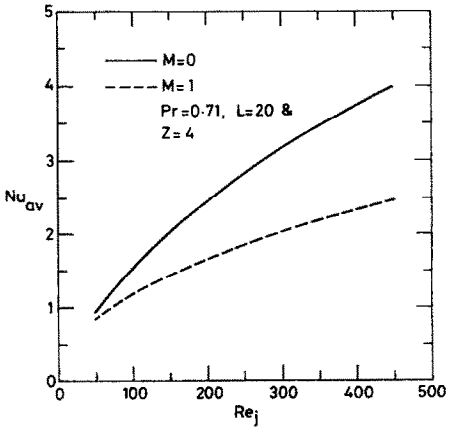

FIG. 8. Average Nusselt number variation with jet-Reynolds-number; semi-confined-jet impingement without and with crossflow.

Table 1. Heat-transfer correlations for laminar slot-jet impingement on a flat surface; unchanged parameters assume the default values: $Re_j = 200$, $Pr = 0.71$, $L = 20$, $Z = 4$ and $M = 0$ and 1

No.	Correlation	Remarks	Range	Figure
1	$Nu_{av} = 0.08Re_j^{0.65}$	$M = 0$	$50 \leqslant Re_j \leqslant 450$	8
2	$Nu_{av} = 0.13Re_j^{0.48}$	$M = 1$	$50 \leqslant Re_j \leqslant 450$	8
3	$Nu_{av} = 2.45Pr^{0.40}$	$M = 0$	$0.1 \leqslant Pr \leqslant 100$	9
4	$Nu_{av} = 1.82Pr^{0.37}$	$M = 1$	$0.1 \leqslant Pr \leqslant 100$	9
5	$Nu_{av} = 12.3L^{-0.53}$	$M = 0$	$6.5 \leqslant L \leqslant 20$	10
6	$Nu_{av} = 6.20L^{-0.44}$	$M = 1$	$6.5 \leqslant L \leqslant 20$	10
7	$Nu_{av} = 2.84Z^{-0.18}$	$M = 0$	$1.0 \leqslant Z \leqslant 2.5$	11
8	$Nu_{av} = 2.30Z^{0.04}$	$M = 0$	$2.5 < Z \leqslant 5.0$	11
9	$Nu_{av} = 2.88Z^{-0.09}$	$M = 0$	$5.0 < Z \leqslant 16$	11
10	$Nu_{av} = 3.25Z^{-0.46}$	$M = 1$	$1.0 \leqslant Z \leqslant 16$	11
11	$Nu_{av} = 1.43M^{-0.08}$	Default parameters	$0.25 \leqslant M \leqslant 0.5$	12
12	$Nu_{av} = 1.70M^{0.23}$	Default parameters	$0.5 \leqslant M \leqslant 6$	12
13	$Nu_{av} = 1.96M^{-0.19}$	$Re_j = 450$	$0.25 \leqslant M \leqslant 0.5$	12
14	$Nu_{av} = 2.52M^{0.21}$	$Re_j = 450$	$0.5 < M \leqslant 6$	12
15	$Nu_{av} = 1.83M^{-0.15}$	$L = 10$	$0.25 \leqslant M \leqslant 0.5$	12
16	$Nu_{av} = 2.32M^{0.22}$	$L = 10$	$0.5 < M \leqslant 6$	12
17	$Nu_{av} = 1.16M^{-0.25}$	$Z = 8$	$0.25 \leqslant M \leqslant 0.75$	12
18	$Nu_{av} = 1.25M^{0.18}$	$Z = 8$	$0.75 < M \leqslant 6$	12

the present parameters, Nu_{av} are correlated to Re_j to the powers 0.65 and 0.48 for $M = 0$ and 1, respectively. These results are given in Table 1 by correlations (1) and (2).

(c) *Effects of Prandtl number on average Nusselt number*

Figure 9 presents the variation of Nu_{av} with Pr and, also, shows the crossflow effects. It is interesting to note the sharp increase in Nu_{av} with increasing Pr at small values of the latter. The reduction in Nu_{av} due to crossflow is about 33% of the nominal values and is about constant over the entire range of Pr investigated. This is reflected in the proximity of exponents in Pr which correlate Nu_{av} (0.40 and 0.37 for $M = 0$ and 1, respectively). These are given by correlations (3) and (4) in Table 1.

(d) *Effects of heat-transfer surface length on average Nusselt number*

Figure 10 illustrates the variation of Nu_{av} with L for the two cases of without and with crossflow. The Nu_{av} decreases with increasing L since the favourable jet-impingement characteristics are localized on the plate area close and under the slot-jet exit, as was shown in Fig. 6. The reduction in Nu_{av} due to crossflow is about 37% of the nominal values. Correlations (5) and (6) in Table 1 relate Nu_{av} to L for $M = 0$ and 1. It follows that when the heat-transfer surface is relatively long with respect to the slot width, it would probably be advantageous to locate more than one slot-jet, say a row of slot-jets, at appropriate spacings above the heat-transfer surface. A complicated crossflow interaction would arise but it is

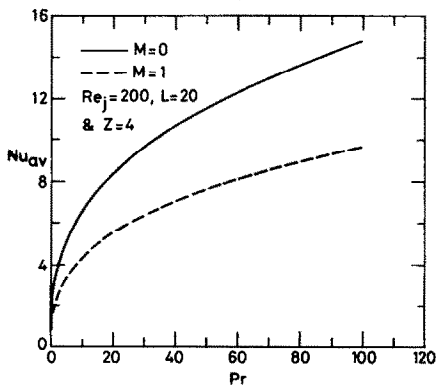

FIG. 9. Average Nusselt number variation with Prandtl number; semi-confined-jet impingement without and with crossflow.

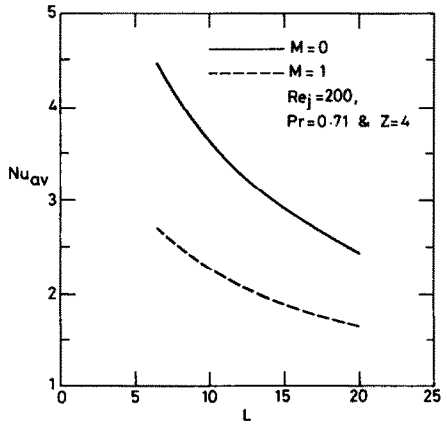

FIG. 10. Average Nusselt number variation with heat-transfer surface length; semi-confined-jet impingement without and with crossflow.

expected that the heat-transfer rate per unit mass of issuing jets would increase.

(e) *Effects of separation distance on average Nusselt number*

Figure 11 depicts the effects of the separation distance between the slot-jet exit plane and impingement surface (Z) on the surface average Nusselt number. For small separation distances, $Z < 2$, the calculations show relatively large Nu_{av}. This is attributed mainly to the resulting high parallel-to-plate velocity as a consequence of the mass continuity requirement and the small area available to flow in between the two parallel plates. In such a situation, the jet impingement behaviour is being overwhelmed by a dominant parallel-to-plate flow over the heated region.

In the absence of a crossflow and for the parameters studied, Nu_{av} is not being much affected by Z for $Z > 2.5$; an optimum Nu_{av} is calculated at about $Z = 5$. A very gradual decrease in Nu_{av} then follows with increasing Z. In the presence of a crossflow, on the other hand, a substantial decrease in Nu_{av} results with increasing Z. At $Z = 4$, the reduction in Nu_{av} is about 30%; and at $Z = 16$, the reduction increases to about 60% of the nominal values. Accordingly, in the presence of a crossflow and as is dictated by the physical situation, Z should not be increased unnecessarily. Correlations (7)–(10) in Table 1 summarize these relations; the weak dependence of Nu_{av} on Z for $M = 0$ and $Z > 2.5$ is reflected by the small exponents of Z.

(f) *Effects of crossflow-to-jet mass-flow-rate ratio on average Nusselt number*

Figure 12 displays the variation of Nu_{av} with M. The solid curve is constructed with the default values of parameters and is used as a datum for comparing other results with different Re_j, L and Z. The smallest non-zero M investigated is equal to 0.25; the curves

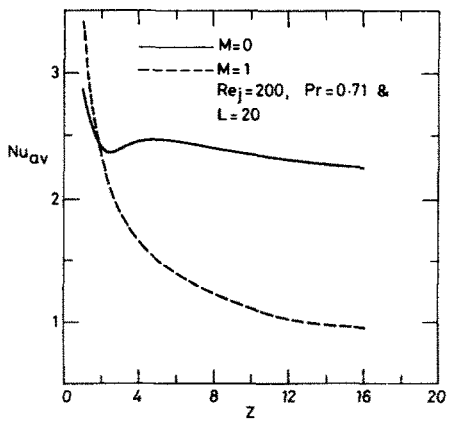

FIG. 11. Average Nusselt number variation with separation distance between slot-jet exit plane and impingement surface; semi-confined-jet impingement without and with crossflow.

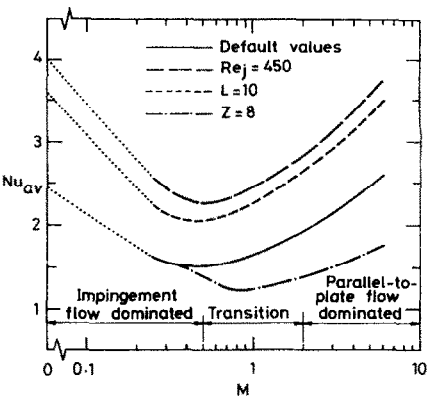

FIG. 12. Average Nusselt number variation with crossflow-to-jet mass-flow-rate ratio; semi-confined-jet impingement showing effects of Re_j, L and Z, other parameters are set at default values.

are extended by dotted straight lines to Nu_{av} values obtained without a crossflow ($M = 0$).

All the results share the same general trend of variation in the sense that Nu_{av} exhibits a maximum value at $M = 0$ and a minimum at $M \approx 0.5$. The minimum Nu_{av} is about 60% of its maximum nominal value obtained without a crossflow. At M greater than about 0.5, Nu_{av} increases with increasing M and continues so as long as the crossflow velocity keeps increasing. It follows that a crossflow-to-jet mass-flow-rate ratio of about 0.5 marks a turning point between two distinguished flow and heat-transfer situations. The first situation (or zone), where M is less than about 0.5, is dominated by jet-impingement flow characteristics and in which the heat-transfer rate deteriorates with increasing M. The second situation (or zone), where M is greater than about 0.5, is dominated by parallel-to-plate crossflow characteristics and in which the heat-transfer rate increases with increasing M. The start of this gradual 'hand over' in behaviour from jet impingement dominated flow to crossflow dominated flow, as M increases, can clearly be seen in Fig. 6. An overlapping or transition zone is roughly estimated at $0.5 \leqslant M \leqslant 2$.

As to the comparisons between the various curves on Fig. 12, it is interesting to note that increasing Re_j has practically the same effect on Nu_{av} as decreasing L (the top two curves). It is also worth noting the insensitivity of Nu_{av} to Z for M values below about 0.5 (the bottom two curves), as was remarked earlier and seen in Fig. 11 for $M = 0$. Increasing Z, on the other hand, increases the value of M for the minimum Nu_{av}; for $Z = 8$, the minimum Nu_{av} is calculated at $M \approx 0.75$. Correlations (11)–(18) in Table 1 give the relations between Nu_{av} and M for the parameters studied.

4.6. *Heat-transfer correlations*

For the range of parameters investigated in the present study, Table 1 contains a summary of the power-fit relations that correlate the average Nusselt

number with the various parameters. Each correlation relates Nu_{av} to only one individual parameter; the rest of the parameters are set at the default values. The results have already been presented in Figs. 8–12. In general and for $M = 0$, Re_j is correlated with a 0.65-power dependence; Pr is correlated with a 0.4-power dependence; L is correlated with -0.53-power dependence and, for $Z > 5$, Z is correlated with a -0.09-power dependence. For $M = 1$, Re_j is correlated with a 0.48-power dependence; Pr is correlated with a 0.37-power dependence; L is correlated with a -0.44-power dependence and Z is correlated with a -0.46-power dependence.

5. CONCLUSIONS

A mathematical model for evaluating the behaviour of steady, laminar and two-dimensional jets impinging on hot flat surfaces was constructed. The model uses a control-volume finite-difference iterative method.

The model was applied for the evaluation of the flow and thermal characteristics of jet impingements for three cases; namely, free-jet impingement, semi-confined-jet impingement and semi-confined-jet impingement with crossflow effects.

The computed results were compared with available experimental measurements, for the case of a free-jet impingement, and the agreement was found to be very good. This demonstrated the accuracy and validity of the model.

A parametric study was conducted to investigate the effects of varying the influential parameters and of imposing a crossflow on the impingement characteristics. The average Nusselt number was correlated with the various parameters.

For the range of parameters investigated, the following major findings may be summarized.

The Nusselt number variation along the heat-transfer surface shows an enhanced heat-transfer rate at the impingement region.

The heat-transfer characteristics along the impingement region are found to be very sensitive to the velocity distribution at the slot-jet exit. A fully developed parabolic velocity distribution produces Nusselt number values, at the impingement region, that are much higher than those produced by a uniform velocity profile.

The free and semi-confined jet impingements show practically identical results at and near the impingement region. Slight differences are calculated away from this region due to entrainment effects.

The average Nusselt number increases with the increase in the jet-Reynolds-number and the fluid Prandtl number; it decreases with the increase in the length of the heat-transfer surface and the separation distance between the jet-exit and the impingement surface.

The presence of a crossflow degrades the favourable characteristics of impinging jets, and can reduce the nominal Nusselt number by as much as 60%.

A crossflow-to-jet mass-flow-rate ratio of more than about two alters the nature of the problem from being dominated by a jet-impingement behaviour to a parallel-to-plate crossflow dominated.

REFERENCES

1. R. Gardon and J. C. Akfirat, Heat transfer characteristics of impinging two-dimensional air jets, *Trans. ASME J. Heat Transfer* **88,** 101–108 (1966).
2. M. Korger and F. Krizek, Mass-transfer coefficient in impingement flow from slotted nozzles, *Int. J. Heat Mass Transfer* **9,** 337–344 (1966).
3. E. M. Sparrow and T. C. Wong, Impingement transfer coefficients due to initially laminar slot jets, *Int. J. Heat Mass Transfer* **18,** 597–605 (1975).
4. J. H. Masliyah and T. T. Nguyen, Mass transfer due to an impinging slot jet, *Int. J. Heat Mass Transfer* **22,** 237–244 (1979).
5. H. Elbanna and J. A. Sabbagh, Flow visualization and measurements in a two-dimensional two-impinging-jet flow, *AIAA J.* **27,** 420–426 (1989).
6. A. D. Gosman, W. M. Pun, A. K. Runchal, D. B. Spalding and M. Wolfshtein, *Heat and Mass Transfer in Recirculating Flows*. Academic Press, London (1969).
7. A. R. P. van Heiningen, A. S. Mujumdar and W. J. M. Douglas, Numerical prediction of the flow field and impingement heat transfer caused by a laminar slot jet, *Trans. ASME J. Heat Transfer* **98,** 654–658 (1976).
8. H. Miyazaki and E. Silberman, Flow and heat transfer on a flat plate normal to a two-dimensional laminar jet issuing from a nozzle of finite height, *Int. J. Heat Mass Transfer* **15,** 2097–2107 (1972).
9. E. M. Sparrow and L. Lee, Analysis of flow field and impingement heat/mass transfer due to a nonuniform slot jet, *Trans. ASME J. Heat Transfer* **97,** 191–197 (1975).
10. S. Mikhail, S. M. Morcos, M. M. M. Abou-Ellail and W. S. Ghaly, Numerical prediction of flow field and heat transfer from a row of laminar slot jets impinging on a flat plate, *Proc. 7th Int. Heat Transfer Conf.*, Vol. 3, pp. 377–382 (1982).
11. T. D. Yuan, J. A. Liburdy and T. Wang, Buoyancy effects on laminar impinging jets, *Int. J. Heat Mass Transfer* **31,** 2137–2145 (1988).
12. V. K. Garg and S. Jayaraj, Boundary layer analysis for two-dimensional slot jet impingement on inclined plates, *Trans. ASME J. Heat Transfer* **110,** 577–582 (1988).
13. L. Y. Cooper, Heat transfer in compartment fires near regions of ceiling-jet impingement on a wall, *Trans. ASME J. Heat Transfer* **111,** 455–460 (1989).
14. S. J. Downs and E. H. James, Jet impingement heat transfer—a literature survey, ASME Paper 87-HT-35 (1987).
15. S. V. Patankar and D. B. Spalding, A calculation procedure for heat, mass and momentum transfer in three-dimensional parabolic flows, *Int. J. Heat Mass Transfer* **15,** 1787–1806 (1972).
16. W. M. Pun and D. B. Spalding, A general computer program for two-dimensional elliptic flows, Report No. HTS/76/2, Dept. of Mech. Engng, Imperial College, London (1976).
17. S. A. Al-Sanea, W. M. Pun and D. B. Spalding, Computation of two-dimensional elliptic flows, including heat transfer, Report No. HTS/78/5, Dept. of Mech. Engng, Imperial College, London (1978), also in *Computer Methods in Fluids* (Edited by K. Morgan, C. Taylor and C. A. Brebbia), pp. 217–256. Pentech Press, London (1980).
18. S. V. Patankar, *Numerical Heat Transfer and Fluid Flow*. Hemisphere, Washington, DC (1980).
19. D. E. Metzger and R. J. Korstad, Effects of crossflow

on impingement heat transfer, *Trans. ASME J. Engng Power* **94**, 35–42 (1972).

APPENDIX: DOMAIN SIZE AND OTHER COMPUTATIONAL DETAILS

It is important that the conditions imposed at the outlet and free-stream boundaries do sufficiently match the assumed developed conditions of the flow (see Section 2.3). Relocating such boundaries further away should not affect the solution in the jet-impingement region. Of particular importance is the accommodation of the top-wall recirculation region, created by the issuing jet, to well inside the calculation domain. The length of the top-wall recirculation region (r), measured from the jet axis, depends on Re_j, Z and M. Figure A1 depicts the variation of R ($=r/b$) with Re_j for the case of a semi-confined-jet impingement with $Z = 4$ and $M = 0$ and 1. For $M = 0$, R is about 6 at $Re_j = 50$; at $Re_j = 450$, R is increased to about 30. With a crossflow, the length of the recirculation region is shortened and becomes a weak function of Re_j; at $Re_j = 450$, R is about 10 for $M = 1$. Figure A2 presents the variation of R with Z for the case of a semi-confined-jet impingement with $Re_j = 200$ and

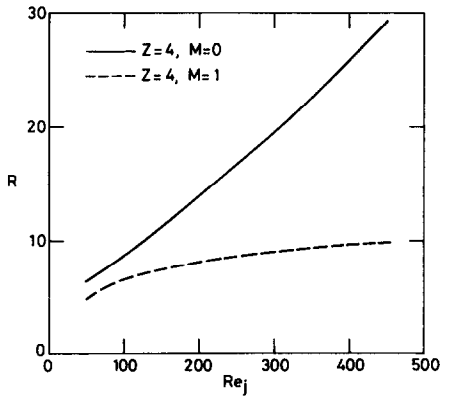

FIG. A1. Length of top-wall recirculation region versus jet-Reynolds-number; semi-confined-jet impingement without and with crossflow.

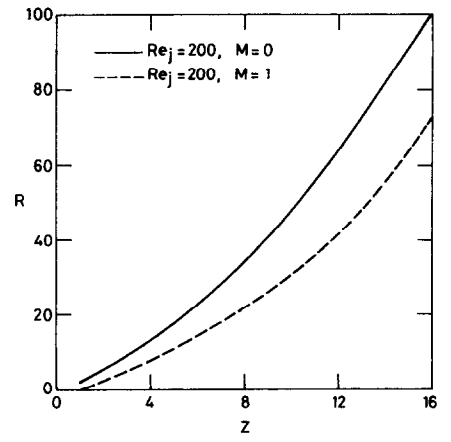

FIG. A2. Length of top-wall recirculation region versus separation distance between slot-jet exit plane and impingement surface; semi-confined-jet impingement without and with crossflow.

$M = 0$ and 1. For $M = 0$, R is about 14 at $Z = 4$; at $Z = 16$, R is increased to about 100. For $M = 1$, R is decreased by about 30% of its value with $M = 0$.

It is found by numerical experiments that a substantially developed flow is attained at about twice the length of the recirculation zone, measured from the jet axis, for the case of a semi-confined-jet impingement without a crossflow. This dictates, with reference to Figs. A1 and A2, where the outlet boundary should be located. In the present study, two sizes of the calculation domain are used; a smaller size ($NX = 40$) with an outlet boundary located at 40 slot widths downstream of the jet axis, and an extended and larger domain ($NX = 50$) with an outlet boundary located at 150 slot widths downstream of the jet axis. The latter domain is constructed by adding 10 more expanding grid lines to the smaller-domain grid and is used for calculations with large Re_j and Z. Table A1 gives the distribution of grid lines for the $NX = 40$ by $NY = 20$ typical grid used for the short domain. In the presence of a crossflow, 20 more grid lines in the x-direction are added to the upstream side of the jet axis to accommodate the crossflow region. The crossflow inlet is situated at 20 slot widths upstream of the jet axis. It is interesting to note that since the crossflow shortens the length of the recirculation region, a shorter domain in the downstream direction could have been used and as is dictated by the results displayed in Figs. A1 and A2.

For the case of a free-jet impingement, the free-stream boundary is located far above the slot-jet exit plane for the flow to assume quiescent free-stream conditions. Numerical experiments, in the range of parameters studied, are conducted to investigate the sensitivity of the results near the impingement surface to the location of the upper free-boundary of the calculation domain. Two locations are employed; the first is situated at twice the distance between the jet-exit-plane and the impingement surface, i.e. at $Y = 2Z$, and the second is situated at $Y = 3Z$. For the two heights considered, the Nu_{av} over $L = 20$ is found to differ by no more than 0.3%, and the maximum difference in Nu is about 1.5% and is calculated at the edge of the heated surface. Therefore, the top boundary is located at an optimum height of $Y = 2Z$. The previous semi-confined-jet impingement grid is, accordingly, enlarged in the y-direction by adding 10 more grid lines above the slot-jet exit plane. In the cases studied with $Z = 4$, fully developed flow conditions are attained at 30 and

Table A1. Typical grid-line distribution; semi-confined-jet impingement without crossflow

IX	X	IX	X	IY	Y
1	0.00	21	7.50	1	0.00
2	0.05	22	8.50	2	0.01
3	0.15	23	9.50	3	0.03
4	0.25	24	10.50	4	0.05
5	0.40	25	11.50	5	0.07
6	0.60	26	13.00	6	0.09
7	0.80	27	15.00	7	0.12
8	1.00	28	17.00	8	0.16
9	1.30	29	19.00	9	0.23
10	1.60	30	21.00	10	0.35
11	1.90	31	23.00	11	0.50
12	2.20	32	25.00	12	0.70
13	2.50	33	27.00	13	1.00
14	3.00	34	29.00	14	1.40
15	3.50	35	31.00	15	1.80
16	4.10	36	33.00	16	2.40
17	4.70	37	35.00	17	3.00
18	5.30	38	37.00	18	3.40
19	5.90	39	39.00	19	3.80
20	6.50	40	40.00	20	4.00

95 slot widths downstream of the jet axis for $Re_j = 50$ and 200, respectively.

The calculations require about 100 kBytes of memory and about 6×10^{-5} s of CPU time per (iteration × variable × grid node × line traverse) on the IBM 3083 machine. Typical converged results are obtained after about 50–150 field iterations; a maximum of three line traverses are used with a typical relaxation factor of 0.5 for all dependent variables.

ETUDE NUMERIQUE DES CARACTERISTIQUES D'ECOULEMENT ET DE TRANSFERT THERMIQUE D'UN JET PLAT LAMINAIRE IMPACTANT AVEC EFFETS DE COURANT CROISE

Résumé—Un modèle numérique basé sur une procédure de volumes finis, est construit et appliqué au calcul des caractéristiques d'écoulement et de transfert thermique permanents pour un jet plat impactant une surface plane isotherme. On étudie les cas suivants: impaction du jet libre, impaction du jet semi-confiné et impaction du jet semi-confiné à travers un courant croisé. Le modèle est validé par comparaison des résultats avec des données expérimentales dans le cas de l'impaction du jet libre; l'accord est trouvé satisfaisant. Une étude paramétrique est conduite en faisant varier les paramètres suivants: nombre de Reynolds du jet, nombre de Prandtl du fluide, longueur de la surface de transfert thermique, distance entre sortie du jet et surface-cible, et dans le cas du courant croisé, rapport des débits de masse du courant croisé et du jet. Le nombre de Nusselt moyen est donné pour les domaines étudiés des paramètres et il est montré que le courant croisé peut dégrader de 60% environ le flux nominal de chaleur transféré.

NUMERISCHE UNTERSUCHUNG VON STRÖMUNG UND WÄRMEÜBERGANG IN EINEM AUFTREFFENDEN LAMINAREN SCHLITZFÖRMIGEN STRAHL UNTER BERÜCKSICHTUNG VON QUERSTRÖMUNGSEFFEKTEN

Zusammenfassung—Mit Hilfe eines numerischen Modells, das auf einem Finite-Volumen-Verfahren beruht, wird die stationäre Strömung und der Wärmeübergang in einem laminaren schlitzförmigen Strahl berechnet, der auf eine isotherme ebene Oberfläche auftrifft. Drei Fälle werden unterschieden: as Auftreffen eines Freistrahls, das Auftreffen eines halbseitig begrenzten Strahls und das Auftreffen eines halbseitig begrenzten Strahles mit Querströmung. Durch Vergleich der Ergebnisse mit verfügbaren Versuchsdaten für den Fall eines Freistrahls wird das Modell validiert, die Übereinstimmung ist sehr gut. Die Einflüsse der folgenden Parameter werden systematisch untersucht: Reynolds-Zahl des Strahls, Prandtl-Zahl des Fluids, Länge der wärmeübertragenden Oberfläche, Abstand zwischen Strahlaustritt und Oberfläche, sowie für den Fall mit Querströmung das Verhältnis der Massenströme der Querströmung und des Strahls insgesamt. Die mittlere Nusselt-Zahl wird für den untersuchten Parameterbereich korreliert, wobie sich zeigt, daß die Querströmung den Wärmeübergang um bis zu 60% vermindern kann.

ЧИСЛЕННОЕ ИССЛЕДОВАНИЕ ХАРАКТЕРИСТИК ТЕЧЕНИЯ И ТЕПЛОПЕРЕНОСА ПРИ НАБЕГАНИИ ЛАМИНАРНОЙ ЩЕЛЕВОЙ СТРУИ С УЧЕТОМ ЭФФЕКТОВ ПОПЕРЕЧНОГО ТЕЧЕНИЯ

Аннотация—На основе метода конечных объемов построена численная модель, которая применяется для расчета характеристик стационарного течения и теплопереноса при набегании ламинарной щелевой струи на изотермическую плоскую поверхность. Исследуются три случая, а именно, набегание свободной струи, набегание полуограниченной струи и набегание полуограниченной струи сквозь поперечный поток. Эффективность модели проверяется сравнением результатов с имеющимися экспериментальными данными для случая набегания свободной струи, и получено очень хорошее согласие. Параметрическое исследование проводится посредством варьирования следующих параметров: числа Рейнольдса для струи, числа Прандтля для жидкости, длины поверхности теплопереноса, расстояния между выходом струи и поверхностью соударения и, в случае поперечного течения, отношения массовых расходов поперечного потока и струи. Среднее число Нуссельта обобщается для исследуемого диапазона параметров. Показано, что поперечный поток может снижать номинальную интенсивность теплопереноса на 60%.